JBC Papers in Press. Published on March 6, 2009 as Manuscript M809164200
The latest version is at http://www.jbc.org/cgi/doi/10.1074/jbc.M809164200

ALANINE SCANNING OF THE S6 SEGMENT REVEALS A UNIQUE AND CYCLIC AMP-SENSITIVE ASSOCIATION BETWEEN THE PORE AND VOLTAGE-DEPENDENT OPENING IN HCN CHANNELS

Vincenzo Macri, Hamed Nazzari, Evan McDonald, Eric A. Accili
From the Department of Cellular and Physiological Sciences, University of British Columbia, Vancouver, BC, Canada, V6T 1Z3

Address correspondence to: Eric A. Accili, Department of Cellular and Physiological Sciences, University of British Columbia, 2350 Health Sciences Mall, Vancouver, BC, V6T 1Z3, Tel. 604-822-6900; Fax. 604-822-6048; Email: eaaccili@interchange.ubc.ca

Hyperpolarization-activated Cyclic Nucleotide-modulated (HCN) channels resemble *Shaker* K^+ channels in structure and function. In both, changes in membrane voltage produce directionally similar movement of positively charged residues in the voltage sensor to alter the pore structure at the intracellular side and gate ion flow. However, HCNs open when hyperpolarized whereas *Shaker* opens when depolarized. Thus, electromechanical coupling between the voltage sensor and gate is opposite. A key determinant of this coupling is the intrinsic stability of the pore. In *Shaker*, an alanine/valine scan of residues across the pore, by single point mutation, showed that most mutations made the channel easier to open and steepened the channel's response to changes in voltage. Because most mutations likely destabilize protein packing, the *Shaker* pore is most stable when closed and the voltage sensor works to open it. In HCN channels, the pore energetics and vector of work by the voltage sensor are unknown. Accordingly, we performed a 22-residue alanine/valine scan of the distal pore of the HCN2 isoform and show that the effects of mutations on channel opening and on the steepness of the channel's response to voltage are mixed and smaller than those in *Shaker*. These data imply that the stabilities of the open and closed pore are similar, the voltage sensor must apply force to close the pore, and the interactions between the pore and voltage-sensor are weak. Moreover, cyclic AMP binding to the channel heightens the effects of the mutations, indicating stronger interactions between the pore and voltage-sensor, and tips the energetic balance towards a more stable open state.

Hyperpolarization-activated Cyclic Nucleotide-modulated (HCN) channels are similar in structure and function to *Shaker* K+ channels (1-3). As in *Shaker*, HCN channels are comprised of 4 subunits which each consist of six predicted membrane-spanning segments (S1-S6). The S1-S4 segments form the voltage-sensing domain, and the S5 and S6 segments, the pore-forming domain. The S4 segment in both channels contains positive charges that move similarly in response to changes in membrane voltage (4-6), to then alter the pore structure at the intracellular side of the S6 segment; this region functions as a voltage-controlled gate to cation flow (7-10). Despite these similarities, HCN channels are opened by hyperpolarization of the membrane potential, whereas *Shaker* channels open in response to depolarization. Thus, the electromechanical coupling between the voltage sensor and the gate is reversed in these two channels.

A key determinant of this coupling is the intrinsic stability of the closed and open conformations of the pore. In *Shaker* channels, it has been proposed that the pore is intrinsically most stable when closed and that the voltage sensor works to open the pore during depolarization (11,12). Results from an alanine/valine scan of residues across the

entire *Shaker* pore, by single point mutation, showed that most mutations made the channel easier to open and steepened the channel's response to changes in voltage. It was argued that because most mutations likely destabilize protein packing, the closed conformation must be the stable state; this is consistent with the observed crystal structures of *Shaker*-related channels KcsA and MthK, in the closed and open states respectively, wherein more optimally and tightly packed helices were seen in the closed conformation (13-15).

Because of presumed shared architecture of the gate between HCN and *Shaker* channels, HCN channels might also be most stable when closed and thus the voltage sensor would work to open the pore upon hyperpolarization. To test this hypothesis, we performed an alanine/valine scan of the C-terminal 22 amino acids of the S6 segment in HCN2, used as a prototype, and examined pore energetics as described previously in *Shaker* (11). Choice of this region for mutation was based on: 1) in *Shaker,* the corresponding region harbors one of two clusters of gating-sensitive residues; and 2) it contains the voltage-controlled gate. Surprisingly, the effects of the mutations on channel opening and on the steepness of the channel's response to voltage are mixed and smaller than those in *Shaker*. These findings imply that, in HCN2, the stability of the open and closed pore are similar, the interactions between the pore and voltage-sensor, both structural and functional, are weaker than in *Shaker*, and that the voltage sensor must apply force to the pore to close it. Thus, *Shaker* is closed and HCN2 is open in the absence of input from the voltage sensor. Moreover, cyclic AMP binding to the HCN2 channel heightens the effects of the mutations, indicating stronger interactions between the pore and voltage-sensor, and tips the energetic balance towards a more stable open state.

EXPERIMENTAL PROCEDURES

Mutagenesis

Single-point alanine/valine mutant HCN2 channels were constructed in one of two ways. First, some mutants were constructed by overlapping PCR mutagenesis using a mouse HCN2 template in pcDNA3.1, as previously described (14). For remaining mutants, base pairs 1172-2216 of the mouse HCN2 template were amplified by PCR primers containing distal EcoRI and BamHI sites and subcloned into pBluescript. Quickchange (Stratagene, La Jolla, CA) was then used to generate mutations in this amplified fragment. Next, BlpI and AgeI digested fragments were inserted into the mouse HCN2 template. All mutations were confirmed via DNA sequencing (NAPS facility, University of British Columbia).

Tissue culture and expression of HCN2 constructs

Chinese hamster ovary (CHO-K1) cells (ATCC, Manassas, VA) were maintained in Hams F-12 media supplemented with antibiotics and 10% FBS (Gibco, Burlington, Ontario), and maintained at 37^{o}C with 5% CO_2. Cells were plated onto glass cover slips. Two days after splitting, mammalian expression vectors encoding wild type or mutant HCN2 channels (2 μg per 35 mm dish), and a green fluorescent protein (GFP) reporter plasmid (0.3 μg per dish), were transiently co-transfected into the cells using the FuGene6 transfection reagent (Roche Biochemical, Indianapolis, IN).

Whole-cell patch clamp electrophysiology

Cells expressing GFP were chosen for whole-cell patch clamp recordings 24-48 hours post transfection. The pipette solution contained (in mM): 130 K-Asp, 10 NaCl, 0.5 $MgCl_2$, 1 EGTA, and 5 HEPES with pH adjusted to 7.4 using KOH. For experiments at saturating levels of cAMP, 2 mM cAMP

(Na salt) was added to the pipette solution. Extracellular recording solution contained (in mM): 135 KCl, 5 NaCl, 1.8 $CaCl_2$, 0.5 $MgCl_2$, and 5 HEPES with pH adjusted to 7.4 using KOH. Whole-cell currents were recorded using an Axopatch 200B amplifier and Clampex software (Axon Instruments, Union City, CA) at room temperature. Patch clamp pipettes were pulled from borosilicate glass and fire polished before use (pipette R= 2.5-4.5 MΩ).

Data analysis

Data were filtered at 2 kHz and were analyzed using Clampfit (Axon Instruments, Union City, CA), Origin (Microcal, Northhampton, MA) and Excel (Microsoft, Seattle, WA) software. I_f activation curves were determined from tail currents at a 2 s pulse to -35 mV following 3 to 15 s test pulses ranging from -150 mV to -10 mV, in 20 mV steps. Single tail current test pulses were followed by a 500 ms pulse to +5 mV to ensure complete channel deactivation. The resting current was allowed to return to its baseline value before subsequent voltage pulses. I_f activation curves were determined by plotting normalized tail current amplitudes versus test voltage and fitting these with a single order Boltzmann function,

$$f(V) = I_{max}/(1 + e^{(V½-V)/k}) \qquad \text{(Eq. 1)}$$

to determine the midpoint of activation (V½) and slope factor (k). The effective charge (Z) was calculated using the equation Z = RT/kF, where T = 295K and R and F have their usual thermodynamic meanings. Changes in free energy between open and closed states were given by -ZFV½. The perturbation in free energy produced by introduction of the point mutations (Δ(ZFV½)) was given by $-F(Z_{mut}V½_{mut} - Z_{wt}V½_{wt})$. The standard errors for Δ(ZFV½) were calculated using $\alpha_{\Delta(ZFV½)} = (\alpha^2_{ZFV½,wt} + \alpha^2_{ZFV½,\,mut})^{1/2}$.

Differences in values for V½, Z and ZFV½ between the wild type channel and mutant channels were determined independently using an unpaired t-test ($P<0.05$ was considered significant).

Western Blot Analysis

Each sample was derived from cells on 35mm plates that had been lysed in 100 µL of lysis buffer containing 50mM Tris at pH 8.0, 1% NP40, 150mM NaCl, 1mM EDTA, 1mM PMSF, 2mM each of Na_3VO_4 and NaF, and 10µg/mL each of aprotinin, pepstatin, and leupeptin. Samples were left on ice for 30 minutes, during which time they were vortexed every 5 minutes for ~5 s. After centrifugation to remove cell debris (25,000g, 25 minutes), protein concentration of the supernatant was determined by Bradford assay. 20 µg samples of supernatant were fractionated by sodium dodecyl sulphate-polyacrylamide gel electrophoresis (SDS-PAGE, 8%) and electroblotted to polyvinylidene fluoride (PVDF) membrane (Bio-Rad, Mississauga, ON). Blots were washed three times in TBST (50 mM Tris, pH 7.4, 150 mM NaCl, 0.1% Tween 20) and then blocked with 5% non-fat dry milk (Bio-Rad) in TBST for 1 hour at room temperature. Blots were then incubated with a rabbit polyclonal antibody specific to the C-terminus of HCN2 (Affinity Bioreagents, Golden, CO), at a dilution of 1:500 in TBST with 5% non-fat dry milk for 2.5 hours at room temperature. Blots were washed in TBST for 10 minutes, three times, and then incubated with horseradish peroxidase conjugated to goat anti-rabbit 1:3000 dilution in 5% non-fat dry milk with TBST for 1 hour at room temperature; they were subsequently washed 3 times in TBST. Signals were obtained with ECL Western Blotting Detection Reagents (GE Healthcare, Baie d'Urfe, QC). Protein loading was controlled by probing all Western blots with goat anti-GAPDH antibody (Santa Cruz Biotechnology, Santa Cruz, CA).

RESULTS

Alanine/valine scanning of the distal S6 reveals small changes in perturbation energy

To determine the most stable conformation of the channel, we performed a single-point alanine/valine scan of the C-terminal 22 amino acids of the S6 segment in HCN2 (I422-D443) and examined channel opening, as described previously in *Shaker* (11). We hypothesized that, as for *Shaker* channels, the values for V½ would be shifted in the positive direction and Z would be larger, due to disruption of a more stable closed state by introduced alanine or valine residues. This assumes that the closed conformation of the channel is at an energetic minimum, and that all of the mutations within the S6 will result in positive perturbation energies. The S6 sites involved in positive perturbations promote a more stable closed conformation whereas those that produce negative perturbations promote a more stable open conformation. The relative numbers that shift in the two directions give an approximation of the relative stability of the open versus the closed conformations e.g. a larger number of negative perturbation energies would suggest a more stable open state, an equal number of positive and negative perturbation energies would suggest that the stabilities of the open and closed conformations are about equal. Finally, this assumes that each residue contributes equally to stability.

Wild type and mutant channels were expressed independently in CHO cells from which I_f was recorded using the whole-cell patch clamp approach. I_f activation curves were determined by plotting normalized tail current amplitudes versus test voltage and fitting these with Equation 1 (Experimental Procedures). From this fit, values for V½ and Z were determined to thereby allow calculation of perturbation energies (Table 1A,B). Gating parameters and perturbation energies of wildtype channels were compared to those of the mutant channels using an unpaired t-test. Eighteen of 22 single-point mutations expressed measurable levels of I_f from which activation curves could be derived (Fig. 1A,B). Levels of I_f for G424A, A425V, T426A, and Y428A were not detectable. Unexpectedly, more mutants had a V½ value that were either significantly more negative (5/18) or unchanged (10/18) from that of wild type, than those which were more positive (3/18) (Fig. 1C, upper). With one exception, all Z values of mutants were unchanged from that of wild type (Fig. 1C, lower). Finally, with the exception of three values, the free energies of mutants were unchanged from that of wild type (Fig. 1D). The mix of positive and negative shifts in V½, and lack of change in free energies in the mutant channels suggest that, contrary to our hypothesis, the stabilities of the open and closed conformations are similar. These data are in accordance with recent findings from an alanine/valine scan of the S6 in HCN2 expressed in *Xenopus* oocytes, which showed that most mutations shifted the opening of the channel to more negative potentials or had no effect; however, the energetic repercussions of these changes on gating were not explored (16).

Cyclic AMP shifts the balance of perturbation energies of the S6 mutations toward negative values

Cyclic AMP stabilizes the open conformation of HCN channels by removing a tonic inhibitory action of the cyclic nucleotide-binding domain (CNBD), located in the C-terminus, on pore opening (17-22). Inhibition by the CNBD occurs by a coupled interaction with the C-linker, a structure that connects the CNBD to the S6 helices, which is thought to apply a force on these helices to inhibit pore opening (20,23). Cyclic AMP binding reverses the coupled interaction which then alleviates inhibition of pore

opening thereby promoting a more stable open state. Given a more stable open conformation upon cAMP binding, we hypothesized that, in saturating levels of this cyclic nucleotide, the S6 mutations would produce more dramatic effects on V½ and Z, and a shift in perturbation energies towards more negative values.

To test this hypothesis, identical experiments were conducted with all 22 mutant channels and the wild type channel at saturating levels of cAMP (2 mM). All but one mutant (G424A) expressed measurable levels of I_f from which activation curves could be determined (Fig. 2A, B). For the wild type HCN2 channel, V½ was shifted +10.1 mV and Z was decreased 0.4 compared to the values determined at basal cAMP (Table 1A,B). The majority of V½ values in the mutant channels were more negative (6/21) or unchanged (9/21) compared to wild type, whereas fewer values were more positive (6/21) (Fig. 2C, upper). The majority of Z values were larger (6/21) or unchanged (14/21) compared to wild type, whereas only one value was smaller (Fig. 2C, lower). A majority of free energies were more negative (9/21) or unchanged (11/21) compared to wild type, but only one value was more positive (Fig. 2D).

Comparing free energies in saturating cAMP with those in basal cAMP (Fig. 1D and Fig. 2D), there was a lower proportion of more positive free energies (1/21 versus 2/18), a lower proportion of unchanged free energies (11/21 versus 15/18) and a higher proportion more negative free energies (9/21 versus 1/18). For one site (G433A), free energy was significantly positive in basal cAMP but, in saturating concentrations of cAMP, it was not altered significantly. The shift of perturbation energies towards the negative, when assayed at saturating levels of cAMP, suggest that the open conformation becomes more stable as a result of cAMP binding.

Three of the mutants that were not functional in basal cAMP recovered function in saturating levels cAMP (A425V, T426A and Y428A), which may have been due to one or both of the following reasons. First, in basal cAMP levels, the mutations may have shifted the range of current activation to very negative voltages at which function cannot be reliably ascertained (i.e. more negative than -150 mV). In elevated cAMP, the activation range would have moved to less negative voltages where the likelihood of detecting channel activity is increased using our protocols. Second, the number of functional channels at the cell surface or single channel conductance may have been reduced by the mutations. For HCN2 channels, cAMP has been suggested to increase open probability in addition to shifting the activation curve to more positive voltages (20), which could have overcome reductions in number of functional channels or single channel conductance. A reduction in the number of functional channels or single channel conductance by these three mutations is supported by the significantly lower levels of current they produce compared to the wild type channel (wt HCN2, -421 ± 98 pA/pF, n= 8; A425V, -71 ± 8 pA/pF n = 3; T426A, -116 ± 22 pA/pF, n = 4; Y428A, -100 ± 16 pA/pF, n = 5; all of the mutants are significantly different from wild type HCN2, $p<0.05$).

The G424A mutant did not yield current in either basal or elevated cAMP. A lack of function has also been reported for the identical mutant when expressed in *Xenopus* oocytes (16). Western blotting showed that this mutant did not undergo complex glycosylation, unlike the wild type channel but like a channel in which the N-glycosylation site has been mutated (N380Q) (Fig. 3). These data suggest that G424 is important for plasma membrane localization of functional channels.

The effects of S6 mutations on Z are consistent with an altered closed to open transition

In *Shaker*, an alanine/valine scan of the pore showed that Z values increased as V½ values became more negative (11). This relationship is consistent with effects on the final closed to open step in a linear gating scheme in which each of the four voltage sensors moves independently and, once all sensors reach the permissive state, the pore opens by a voltage-independent concerted transition (24,25).

For HCN2, we were struck by the mutation-induced changes in Z because they were very small compared to those in *Shaker*. To determine whether the comparatively small changes in Z are still consistent with an altered closed to open step in HCN2, we applied an allosteric model that captures most aspects of HCN channel gating behavior (26).

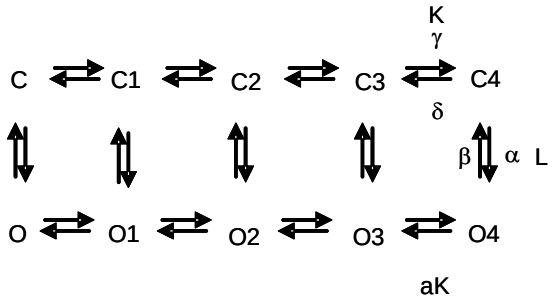

In this model, the voltage sensor in each of the four monomeric subunits moves from reluctant to willing states (C to C4) independently to then allosterically trigger closed to open transitions. Successive engagement of each subunit enhances the probability of channel opening (P_o) given by

$$P_o = \frac{1}{1 + L(V)\left(\frac{1+1/K(V)}{1+1/aK(V)}\right)^4} \qquad \text{(Eq. 2)}$$

where K(V) and L(V) are the equilibrium constants for voltage sensor movement and the closed to open step, respectively. One important way in which this model differs from the scheme used to describe *Shaker* is that the closed to open step is dependent upon voltage. Using this model, Altomare et al (2001) showed that HCN-mediated currents were well-fitted, and that isoform-specific positions of the activation curves and delays in both current activation and deactivation could be predicted.

We used this allosteric model to generate hypothetical values of Z and V½ by varying the rate of either the closed to open step (L(V)) or voltage-sensor movement (K(V)) to assess which change could best predict the effects of the S6 mutations on Z. Because the HCN2 S6 mutations are in a region of the pore that contains the gate, an effect on the closed to open transition, and thus on L(V), would be expected. Z values derived from model P_o curves by varying L(V), but not by varying K(V), should then approximate our experimental Z values.

To test this, P_o curves were generated using Eq. 2 with a range of L(V) and K(V) values and model parameters specific for either basal or 2 mM cAMP. Model parameters were determined by best fitting and are shown in Table 2. Select P_o curves that spanned a similar range of voltages as those determined experimentally were then fitted with Eq. 1 to yield theoretical values for Z and V½, which were then plotted in Fig. 4A and 4B. Both the Z values obtained by varying L(V) and those observed experimentally do not vary greatly with V½; this held true at basal and at saturating levels of cAMP (in Fig. 4, compare the experimentally determined Z values with those determined from the model using a range of L(V) values, represented by the individual symbols and the black lines, respectively). In contrast, the Z values obtained by varying K(V) in the model

increase at more negative voltages and plateau in range of voltages separate from that in which most of the experimentally determined Z values are found, in both basal and saturating levels of cAMP (in Fig. 4, compare the experimentally determined Z values with those determined from the model using a range of K(V) values, represented by the individual symbols and the gray lines, respectively). Furthermore, when K(V) was decreased in the model, the activation curves reached a point at which Z and V½ values changed very little, even with very small values for K(V). Consequently, there are no model Z values at voltages less negative than ~-95 mV in Fig. 4 (note that the gray lines do not continue to less negative voltages in this Figure). These data are consistent with an impact of the S6 mutations primarily on L(V) and thus on the closed to open transition.

However, some Z values were affected significantly by the mutations, especially when cAMP was elevated (note the colored points in Fig. 4). This is not predicted by the model when varying either L(V) or K(V), suggesting that combined effects of the mutations on both voltage sensor movement and the closed to open step, and/or on other transitions prior to the final steps, contribute significantly to the observed changes in Z.

DISCUSSION

The mixed effects on the voltage-dependence of channel opening and very small perturbation energies produced by the majority of S6 mutations in basal levels of cAMP, and an abundance of mutations with negative perturbation energies in saturating levels of cAMP, suggest that the stability of the open and closed states are similar, and that cAMP binding shifts the energetic balance toward a more stable open state. This implies that the voltage sensors must apply force upon the HCN2 pore to close. This is unlike *Shaker* channels, which are most stable in the closed conformation and in which voltage sensor works to open the pore (11). Thus, voltage-dependent channel gating in both HCN and *Shaker* channels is constrained such that the force exerted by the voltage sensor on the gate occurs during depolarization of the membrane potential.

Our findings explain the presence of an "instantaneous" current at all voltages in wild type HCN channels (3,27-30), and the frequent observation that artificial perturbations to HCN lead to even larger constitutively-active currents. A resting conductance of ~2% has been estimated for HCN2 channels, whereas a value between 4-8% has been estimated for sea urchin HCN channels, without and with cAMP, respectively (28). Our data imply that the channel open probability does not reach zero, yielding a significant resting conductance, and that the voltage sensor is unable to exert sufficient force to realize this end. The production of greater constitutive current seen with a number of single-point mutations in the S4-S5 and C- linkers (30-33), and upon cadmium binding to cysteine substitutions near the intracellular side of the pore (8), when understood in the context of a naturally open pore, suggests that these perturbations weaken the link between the voltage sensor and pore. Alternatively, residual current through a channel in the closed state may contribute to a resting conductance but this would not depend upon the energetic balance between the open and closed states. Nevertheless, a constitutively open channel may not necessarily be an inevitable consequence of a pore that is more stable when open. At more positive voltages, the voltage sensor could actively keep the channel shut. This is the opposite of what happens in a channel with a pore that is more stable when closed, like *Shaker*, in which the voltage sensors work to keep the channel open.

Perturbation energies induced by the S6 mutations in HCN2 were smaller than those in *Shaker* (11) which suggest weaker interactions between the voltage-sensing elements and the pore. Loose coupling between the voltage sensor and pore, as might be expected from a weak structural interaction, has been proposed recently for HCN channels (34). These authors showed that the energetics of voltage sensor movement is little affected in sea urchin HCN channels that have been "locked open", as opposed to the energetics of voltage sensor movement in locked open *Shaker* channels which are significantly affected. The lack of apparent coupling in a locked open HCN channel is completely consistent with the notion that the pore is naturally open without input from the voltage sensing elements.

A difference in gating dynamics of HCN2 from *Shaker* is also suggested by our finding that the effective charge Z, determined from the slope of the activation curve, was changed only minimally by the single-point S6 mutations. In contrast, single-point mutations in the S6 of *Shaker* altered Z and perturbation energy to a much greater extent, and the Z values increased as V½ values became more negative (11). This difference in observed Z between these 2 channels may arise from the fact that, in HCN2, the closed to open transition as well as the movement of the voltage sensor may be voltage dependent (11,26). Thus, the slope of the HCN2 activation curve would reflect contributions from both processes, whereas that of *Shaker* would reflect a contribution primarily from voltage sensor movement. It should be noted that in 2007 a study on HCN2 channels suggested that the closed to open transition may instead be voltage independent (21). It will be interesting to determine whether the gating model developed in that study predicts the small changes in Z seen in our study.

Cyclic AMP has been proposed to stabilize the HCN open state by removing an inhibitory action of the CNBD on pore opening. In the absence of cAMP, inhibition by the CNBD occurs by a coupled interaction with the C-linker region that is thought to apply a force on the S6 helices to actively inhibit pore opening (20,23). Our data showing a significant shift of perturbation energies to more negative values by mutations in the S6 are consistent with this proposed action of cAMP and identify a cluster of residues around the proposed activation gate (35) that are modified by the inhibitory action of the CNBD (Supplementary Fig. 1). Our data are also consistent with previous work in sea urchin HCN wherein mutation of a single residue in S6 (F459L) produced an equivalent effect to cAMP on gating (36). The corresponding site in mouse HCN2 (F431) is one of the ten cAMP-sensitive sites identified in our study.

Our data suggest that the primary effect of the S6 mutations is on the closed to open step, the final step of the activation process, which seems reasonable for several reasons. First, the mutations that are energetically sensitive cluster in a region of the S6 that likely forms the activation gate (7,8,35). Second, the small effects of the mutations on effective charge can be mostly, although not completely, explained by effects on the pore opening step. Third, cAMP, which releases the inhibitory influences on pore opening, significantly shifts perturbation energies towards the negative, suggesting that both the mutations and the CNBD target the same region. Nevertheless, an allosteric effect of the mutations on voltage sensor movement could have contributed to the observed alterations in gating. We found that the significant effects on the effective charge (Z) produced by some of the mutations could not be explained by an allosteric model in which only the pore opening step, or only the voltage-sensor movement, was altered. Other strategies are required to determine whether the voltage-sensing elements of HCN channels contribute to the observed effects of the S6 mutations on

gating. It is important to note that the perturbation energies of the S6 mutations in HCN2 are small relative to those in the prototypical *Shaker* channel, especially at basal levels of cAMP; therefore, neither the pore or voltage sensor are apparently affected despite mutations in and around the activation gate. These small perturbation energies, along with their shift toward the negative by cAMP, are strong support for both a weak interaction between the pore and voltage sensor, compared to *Shaker*, and a pore that is not at its energetic minimum when closed. The evidence demonstrating that the effects of the mutations on perturbation energy in saturating cAMP levels are larger, and shifted towards negative, greatly strengthens this conclusion.

A naturally open pore in HCN2 has important implications for the structural orchestration of gating. The direction of charge and voltage sensor movement is similar between HCN and *Shaker*-related channels, despite the inverted dependence of HCN channel opening to voltage, which implies that the coupling of voltage sensor movement to channel opening is inverted (4-6). We suggest that positive force is applied by the voltage sensor to the C-terminal region of the S6 helices during depolarization to cause the gate to close in HCN2, rather than to open as in *Shaker*. The structural details of this action will have to await more sophisticated analyses such as the determination of HCN crystal structure, but we believe our present findings provide a glimpse into a fundamentally different way of cycling between open and closed states in the Kv superfamily of voltage-gated channels.

REFERENCES

1. Santoro, B., Liu, D. T., Yao, H., Bartsch, D., Kandel, E. R., Siegelbaum, S. A., and Tibbs, G. R. (1998) *Cell* **93**(5), 717-729
2. Ludwig, A., Zong, X., Jeglitsch, M., Hofmann, F., and Biel, M. (1998) *Nature* **393**(6685), 587-591
3. Gauss, R., Seifert, R., and Kaupp, U. B. (1998) *Nature* **393**(6685), 583-587
4. Mannikko, R., Elinder, F., and Larsson, H. P. (2002) *Nature* **419**(6909), 837-841
5. Bell, D. C., Yao, H., Saenger, R. C., Riley, J. H., and Siegelbaum, S. A. (2004) *J Gen Physiol* **123**(1), 5-19
6. Vemana, S., Pandey, S., and Larsson, H. P. (2004) *J Gen Physiol* **123**(1), 21-32
7. Shin, K. S., Rothberg, B. S., and Yellen, G. (2001) *J Gen Physiol* **117**(2), 91-101
8. Rothberg, B. S., Shin, K. S., and Yellen, G. (2003) *J Gen Physiol* **122**(5), 501-510
9. Macri, V., Proenza, C., Agranovich, E., Angoli, D., and Accili, E. A. (2002) *J Biol Chem* **277**(39), 35939-35946
10. Giorgetti, A., Carloni, P., Mistrik, P., and Torre, V. (2005) *Biophys J* **89**(2), 932-944
11. Yifrach, O., and MacKinnon, R. (2002) *Cell* **111**(2), 231-239
12. Hackos, D. H., Chang, T. H., and Swartz, K. J. (2002) *J Gen Physiol* **119**(6), 521-532
13. Doyle, D. A., Morais Cabral, J., Pfuetzner, R. A., Kuo, A., Gulbis, J. M., Cohen, S. L., Chait, B. T., and MacKinnon, R. (1998) *Science* **280**(5360), 69-77
14. Jiang, Y., Lee, A., Chen, J., Cadene, M., Chait, B. T., and MacKinnon, R. (2002) *Nature* **417**(6888), 515-522
15. Jiang, Y., Lee, A., Chen, J., Cadene, M., Chait, B. T., and MacKinnon, R. (2002) *Nature* **417**(6888), 523-526
16. Cheng, L., Kinard, K., Rajamani, R., and Sanguinetti, M. C. (2007) *J Pharmacol Exp Ther* **322**(3), 931-939
17. DiFrancesco, D., and Tortora, P. (1991) *Nature* **351**(6322), 145-147

18. DiFrancesco, D. (1999) *J Physiol* **515 (Pt 2)**, 367-376
19. Wainger, B. J., DeGennaro, M., Santoro, B., Siegelbaum, S. A., and Tibbs, G. R. (2001) *Nature* **411**(6839), 805-810
20. Craven, K. B., and Zagotta, W. N. (2004) *J Gen Physiol* **124**(6), 663-677
21. Chen, S., Wang, J., Zhou, L., George, M. S., and Siegelbaum, S. A. (2007) *J Gen Physiol* **129**(2), 175-188
22. Barbuti, A., Baruscotti, M., Altomare, C., Moroni, A., and DiFrancesco, D. (1999) *J Physiol* **520 Pt 3**, 737-744
23. Zhou, L., and Siegelbaum, S. A. (2007) *Structure* **15**(6), 655-670
24. Zagotta, W. N., Hoshi, T., and Aldrich, R. W. (1994) *J Gen Physiol* **103**(2), 321-362
25. Schoppa, N. E., and Sigworth, F. J. (1998) *J Gen Physiol* **111**(2), 313-342
26. Altomare, C., Bucchi, A., Camatini, E., Baruscotti, M., Viscomi, C., Moroni, A., and DiFrancesco, D. (2001) *J Gen Physiol* **117**(6), 519-532
27. Proenza, C., Angoli, D., Agranovich, E., Macri, V., and Accili, E. A. (2002) *J Biol Chem* **277**(7), 5101-5109
28. Proenza, C., and Yellen, G. (2006) *J Gen Physiol* **127**(2), 183-190
29. Ishii, T. M., Takano, M., Xie, L. H., Noma, A., and Ohmori, H. (1999) *J Biol Chem* **274**(18), 12835-12839
30. Chen, J., Mitcheson, J. S., Tristani-Firouzi, M., Lin, M., and Sanguinetti, M. C. (2001) *Proc Natl Acad Sci U S A* **98**(20), 11277-11282
31. Macri, V., and Accili, E. A. (2004) *J Biol Chem* **279**(16), 16832-16846
32. Decher, N., Chen, J., and Sanguinetti, M. C. (2004) *J Biol Chem* **279**(14), 13859-13865
33. Chen, J., Mitcheson, J. S., Lin, M., and Sanguinetti, M. C. (2000) *J Biol Chem* **275**(46), 36465-36471
34. Bruening-Wright, A., Pandey, S., and Larsson, P. (2008) *Biophysical Journal* **94**, 119
35. Rothberg, B. S., Shin, K. S., Phale, P. S., and Yellen, G. (2002) *J Gen Physiol* **119**(1), 83-91
36. Shin, K. S., Maertens, C., Proenza, C., Rothberg, B. S., and Yellen, G. (2004) *Neuron* **41**(5), 737-744
37. Nazzari, H., Angoli, D., Chow, S. S., Whitaker, G., Leclair, L., McDonald, E., Macri, V., Zahynacz, K., Walker, V., and Accili, E. A. (2008) *Am J Physiol Cell Physiol* **295**(3), C642-652
38. Much, B., Wahl-Schott, C., Zong, X., Schneider, A., Baumann, L., Moosmang, S., Ludwig, A., and Biel, M. (2003) *J Biol Chem* **278**(44), 43781-43786

Acknowledgements

VM is the recipient of doctoral scholarships from the Michael Smith Health Research Foundation and the Canadian Institutes for Health Research. HN s the recipient of doctoral scholarships from the Michael Smith Health Research Foundation and the National Sciences and Engineering Research Council of Canada. EAA is the recipient of a Tier II Canada Research Chair. Supported by grants from the Heart and Stroke Foundation of British Columbia & the Yukon (EAA). We would also like to thank Patrick Fletcher for help with Matlab and Martin Biel (Munich) for mouse HCN2 cDNA.

Figure Legends

Figure 1. Alanine scanning of the HCN2 S6 segment minimally perturbs the energetics of channel opening.

A. Current traces recorded from CHO cells expressing wild type and three representative S6 alanine mutant HCN2 channels. Currents were elicited by test voltage pulses ranging from -150 mV to -10 mV, in 20 mV steps from a holding potential of -35 mV. The tail currents were elicited at -35 mV.

B. Representative I_f activation curves determined by plotting tail current amplitudes which were normalized to their maximum value (I/I_{max}), versus test voltages (HCN2, squares; Q440A, circles; C427A, upright triangles; L438A, inverted triangles). The curved lines represent fitting by Eq. 1 (see Experimental Procedures).

C. Bar graphs depicting the changes in V½ (upper) and Z (lower) values for each mutant channel relative to wild type.

D. Bar graph depicting change in perturbation of free energy, Δ(ZFV½), for each mutant channel relative to the wild type channel.

Four mutant channels did not yield measurable levels of I_f (solid line through numbered residue, X axis).

Figure 2. **Saturating levels of cAMP (2 mM) shift the balance of perturbation energies to more negative values.**

A. Current traces recorded from CHO cells expressing wild type and three representative S6 alanine mutant HCN2 channels at saturating levels of cAMP. Currents were elicited by test voltage pulses ranging from -150 mV to -10 mV, in 20 mV steps from a holding potential of -35 mV. The tail currents were elicited at -35 mV.

B. Representative I_f activation curves determined by plotting tail current amplitudes which were normalized to their maximum value (I/I_{max}), versus test voltages (HCN2, squares; Q440A, circles; A437V, upright triangles; T426A, inverted triangles). The curved lines represent fitting by Eq. 1 (see Experimental Procedures).

C. Bar graphs depicting the changes in V½ (upper) and Z (lower) values for each mutant channel relative to wild type.

D. Bar graph depicting change in perturbation of free energy, Δ(ZFV½), in mutant channels relative to wild type.

One mutant channel did not yield measurable levels of I_f (solid line through numbered residue, X axis).

Figure 3. Glycine 424 is critical for the expression of cell surface HCN2 channels.

A. Current traces elicited from cells expressing wild type HCN2 (upper trace) or HCN2G424A (lower trace) in response to hyperpolarizing voltage pulses to -150 mV from a holding potential of -35 mV. B. Western blot probed with a rabbit polyclonal antibody directed against the C-terminus of HCN2. *Lane 1*, untransfected cells (UT), *Lane 2*, wt HCN2, *Lane 3*, HCN2 N380Q (N-glycosylation mutant), *Lane 4*, HCN2-G242A. The arrows indicate the presence of mature (*M*, ~136 kDa), immature (*I*, ~114 kDa) protein forms. These data are representative of 3 independent experiments. Note the absence of a mature form of HCN2 in lanes containing HCN2 N380Q (as demonstrated previously (37,38)) and HCN2 G424A.

Figure 4. Experimental and model Z values are comparable and change minimally over the range of observed mid-activation voltages

Plots of Z values versus V½ values for wild type HCN2 channels and each mutant channel examined, at basal (left) and 2 mM cAMP (right). Each line is derived from paired Z and V½ values determined from model P_o curves at varying L(V) (black) and K(V) (gray) (see Results). Also shown are individual values for Z and V½ obtained experimentally for wild type (filled black diamonds), mutants that are significantly different from wild type (filled red or blue diamonds, which are smaller or larger than wild type, respectively) and mutants that are not significantly different from wild type (open squares).

Table 1A,B. The effects of S6 pore mutations on voltage-dependent gating at basal (A) and saturating (2 mM; B) levels of cAMP

The V½ and Z values are from fits of activation curves with Eq. 1 for wild type and mutant channels (Table 1A, basal cAMP; Table lB, 2 mM cAMP). The free energy of the open or closed state is shown as -ZFV½. The difference in free energy between each mutant channel relative to wild type is indicated by Δ(ZFV½). Data are presented as the mean ± sem. Asterisks represent significant differences from wild type.

Table 2. Allosteric model parameters at basal and saturating (2 mM) levels of cAMP

Parameters were obtained by statistical fitting in Matlab, using those from Altomare et al (2001) as initial values, which were determined for the wild type human HCN2 channel.

Supplementary Figure 1. Distribution of amino acids in distal HCN2 S6 segment that are critical for energetic balance of open and closed configurations

S6 residues with significant perturbation energies (see Table 1) are categorized and mapped according to color on to homology model of the HCN2 pore in the closed state (10). A color key for each residue mutated is shown below. Ten sites, including 2 sites at the N-terminal end and 4 sites at the C-terminal end, were unaffected by the mutations and G424A did not produce current with or without cAMP. A tetramer is shown on the left, whereas the one subunit alone is shown on the right.

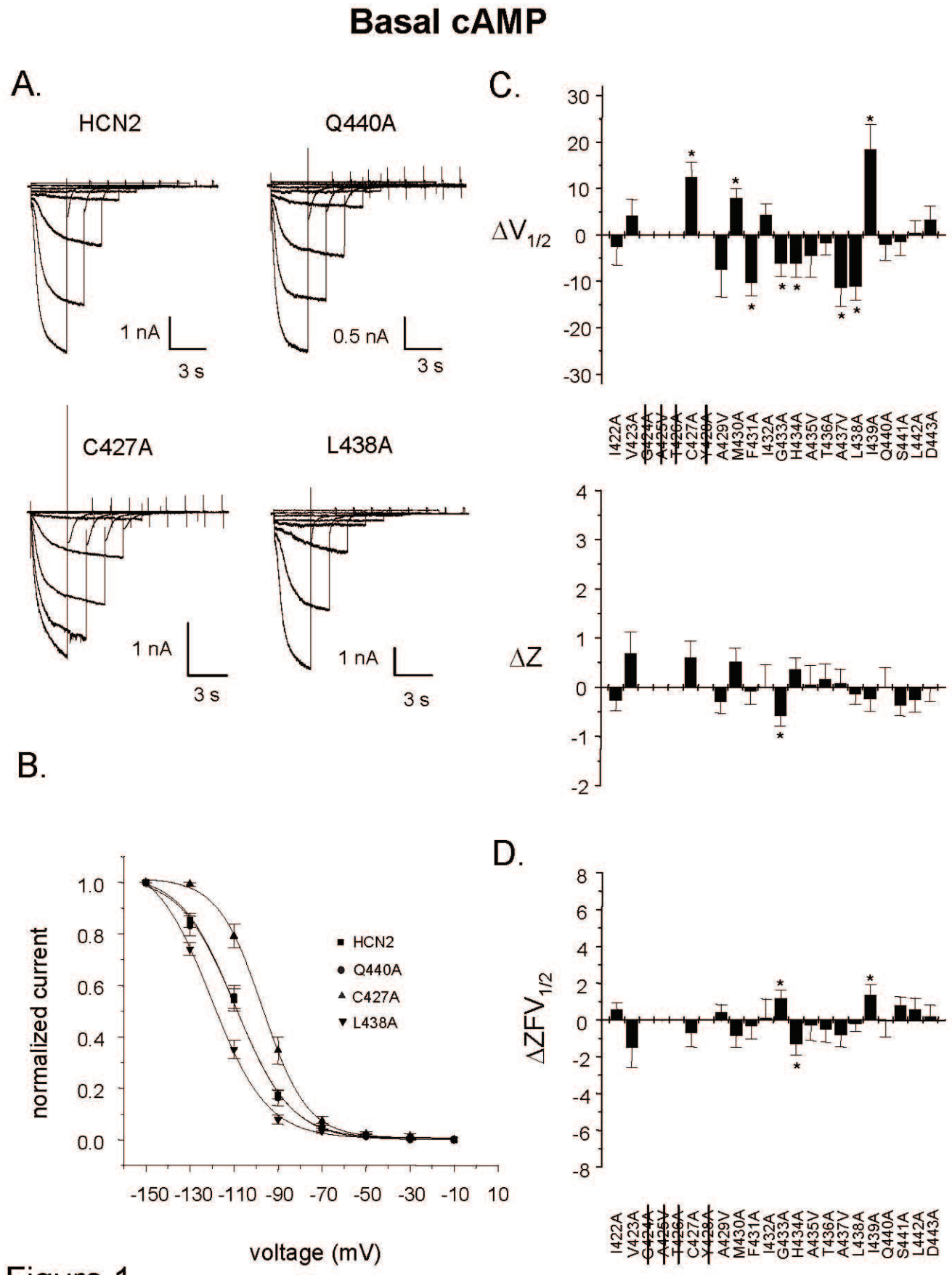

Figure 1

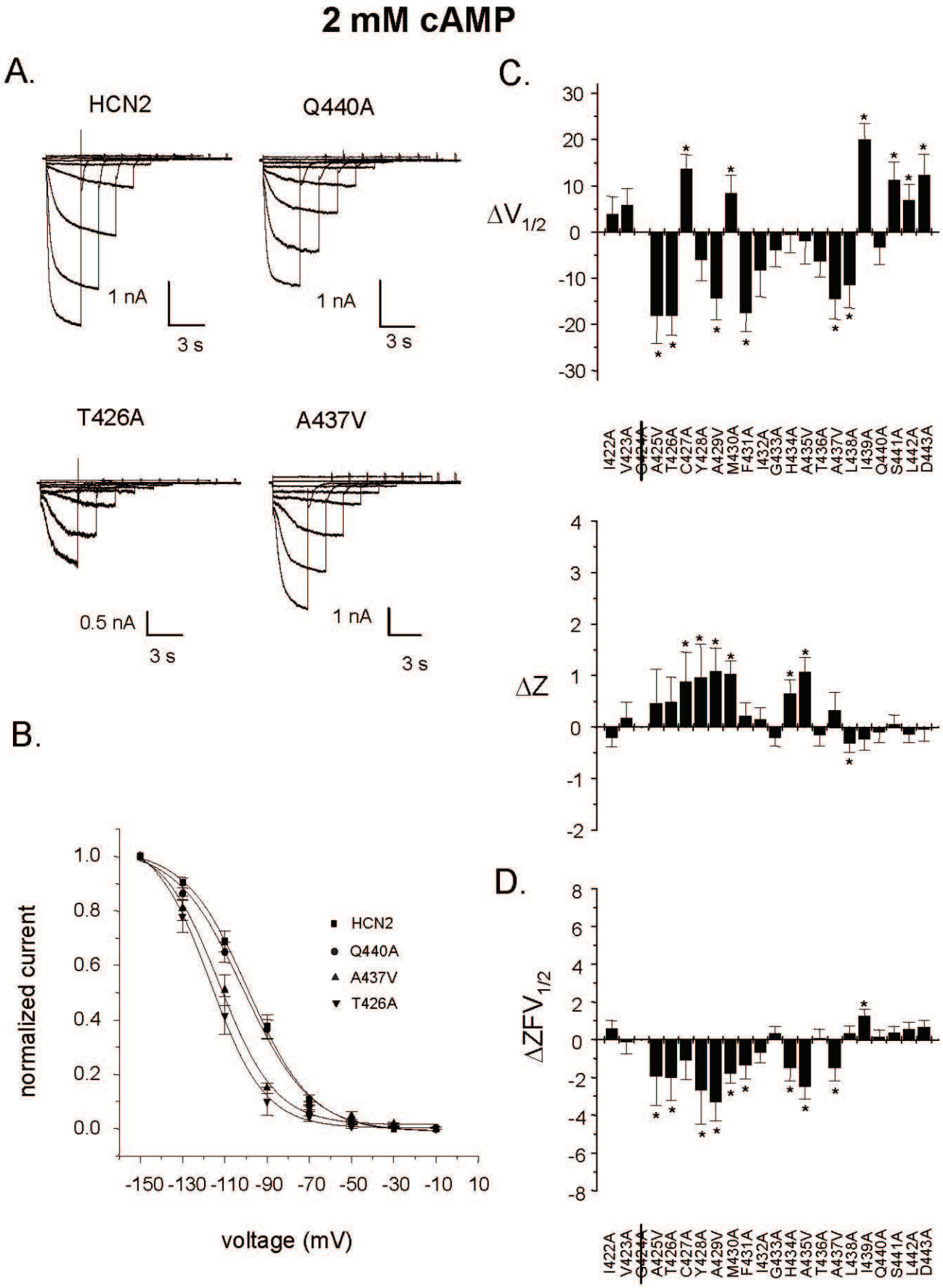

Figure 2

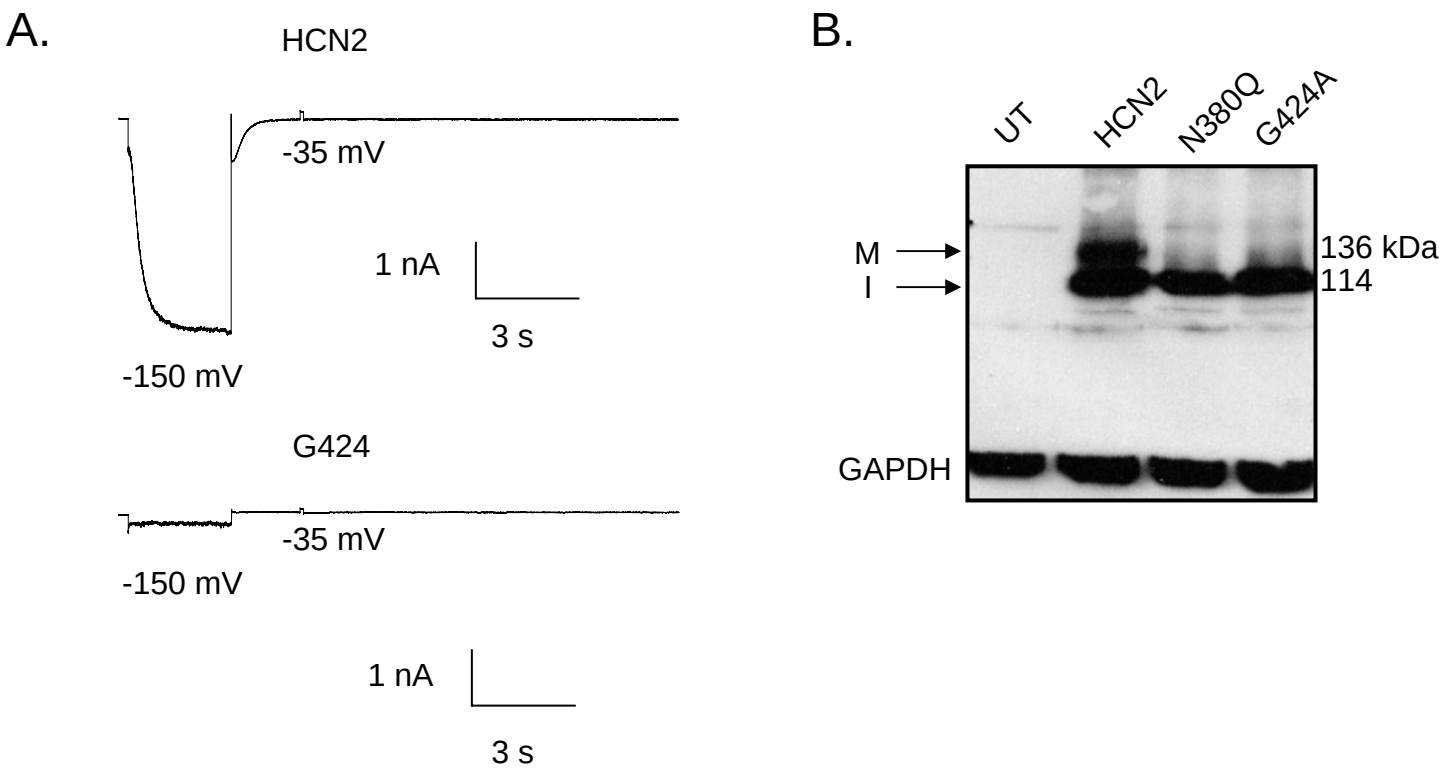
A.
HCN2
-35 mV
1 nA
3 s
-150 mV
G424
-35 mV
-150 mV
1 nA
3 s
B.
UT
HCN2
N380Q
G424A
M
I
136 kDa
114
GAPDH

Figure 3

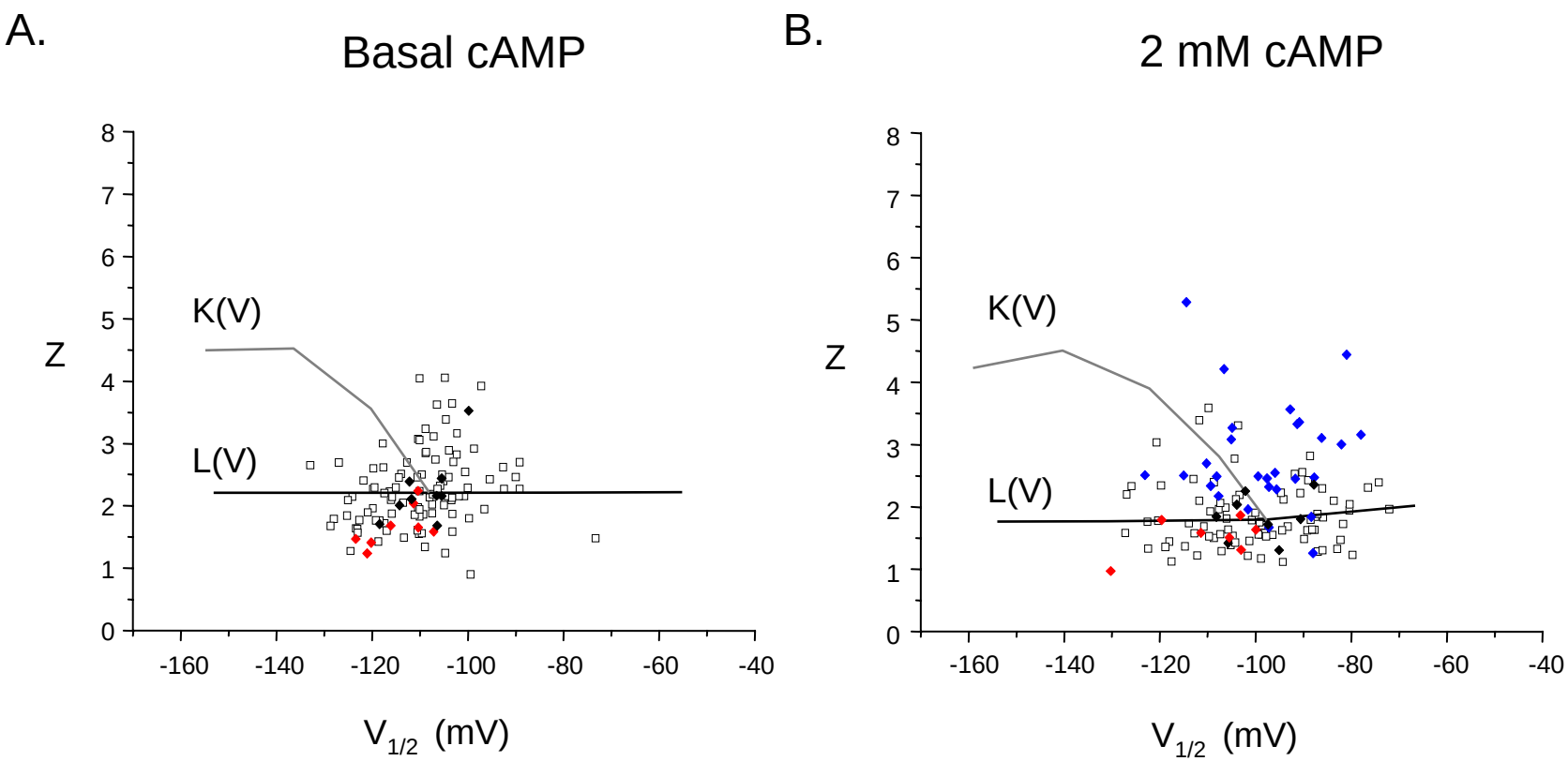
A.
Basal cAMP
B.
2 mM cAMP
K(V)
L(V)
Z
$V_{1/2}$ (mV)
8
7
6
5
4
3
2
1
0
-160
-140
-120
-100
-80
-60
-40

Figure 4

Table 1A

basal cAMP					
HCN2 channel	n	$V_{1/2}$ (mV)	Z	$-ZFV_{1/2}$ (kcal/mol)	$\Delta ZFV_{1/2}$ (kcal/mol)
wild type	9	-108.9 ± 1.8	2.24 ± 0.18	-5.47 ± 0.36	
I422A	6	-111.4 ± 3.4	1.96 ± 0.09	-4.92 ± 0.15	0.54 ± 0.39
V423A	6	-104.7 ± 2.9	2.93 ± 0.40	-6.96 ± 1.03	-1.49 ± 1.09
G424A		no expression			
A425V		no current			
T426A		no current			
C427A	5	-96.4 ± 2.4*	2.85 ± 0.28	-6.20 ± 0.63	-0.73 ± 0.73
Y428A		no current			
A429V	4	-116.4 ± 5.5	1.93 ± 0.12	-5.05 ± 0.18	0.42 ± 041
M430A	4	-101.0 ± 0.84*	2.76 ± 0.22	-6.34 ± 0.51	-0.87 ± 0.62
F431A	5	-119.7 ± 2.0*	2.15 ± 0.18	-5.81 ± 0.57	-0.34 ± 0.68
I432A	5	-104.5 ± 1.3	2.26 ± 0.39	-5.37 ± 0.96	0.11 ± 1.03
G433A	8	-115.0 ± 2.1*	1.66 ± 0.11*	-4.30 ± 0.25*	1.17 ± 0.44
H434A	5	-115.1 ± 2.1*	2.61 ± 0.13	-6.80 ± 0.44*	-1.33 ± 0.57
A435V	5	-113.4 ± 4.2	2.29 ± 0.35	-5.77 ± 0.74	-0.29 ± 0.82
T436A	5	-110.7 ± 1.5	2.40 ± 0.24	-6.00 ± 0.56	-0.53 ± 0.67
A437V	6	-120.2 ± 3.5*	2.32 ± 0.21	-6.28 ± 0.54	-0.81 ± 0.65
L438A	8	-120.1 ± 2.1*	2.09 ± 0.07	-5.67 ± 0.22	-0.19 ± 0.42
I439A	5	-90.4 ± 4.9*	2.00 ± 0.17	-4.12 ± 0.43*	1.35 ± 0.41
Q440A	8	-111.0 ± 2.7	2.25 ± 0.34	-5.55 ± 0.76	-0.08 ± 0.85
S441A	6	-110.4 ± 2.2	1.87 ± 0.11	-4.67 ± 0.27	0.79 ± 0.46
L442A	7	-108.5 ± 1.9	1.99 ± 0.17	-4.89 ± 0.47	0.57 ± 0.61
D443A	6	-105.6 ± 2.2	2.20 ± 0.19	-5.27 ± 0.48	0.19 ± 0.60

Table 1B

2 mM cAMP					
HCN2 channel	n	$V_{1/2}$ (mV)	Z	$-ZFV_{1/2}$ (kcal/mol)	$\Delta ZFV_{1/2}$ (kcal/mol)
wild type	8	-98.8 ± 2.6	1.84 ± 0.13	-4.10 ± 0.28	
I422A	6	-94.9 ± 2.8	1.63 ± 0.11	-3.52 ± 0.32	0.58 ± 0.43
V423A	5	-93.0 ± 2.5	2.02 ± 0.28	-4.22 ± 0.55	-0.12 ± 0.62
G424A		no expression			
A425V	3	-117.0 ± 5.2*	2.30 ± 0.64	-6.03 ± 1.52*	-1.93 ± 1.55
T426A	4	-117.1 ± 3.2*	2.32 ± 0.46	-6.11 ± 1.15*	-2.01 ± 1.19
C427A	5	-85.1 ± 1.5*	2.72 ± 0.55*	-5.18 ± 0.97	-1.07 ± 1.01
Y428A	5	-104.9 ± 3.6	2.80 ± 0.64*	-6.81 ± 1.75*	-2.70 ± 1.77
A429V	4	-113.7 ± 3.7*	2.92 ± 0.42*	-7.43 ± 0.92*	-3.32 ± 0.96
M430A	6	-90.5 ± 2.8*	2.87 ± 0.22*	-5.89 ± 0.42*	-1.79 ± 0.51
F431A	6	-116.3 ± 3.1*	2.06 ± 0.31	-5.45 ± 0.66*	-1.34 ± 0.72
I432A	6	-107.1 ± 5.2	2.00 ± 0.17	-4.77 ± 0.38	-0.67 ± 0.47
G433A	9	-102.7 ± 2.5	1.63 ± 0.09	-3.77 ± 0.22	0.32 ± 0.36
H434A	4	-99.4 ± 2.8	2.49 ± 0.22*	-5.62 ± 0.60*	-1.52 ± 0.67
A435V	4	-100.7 ± 4.2	2.91 ± 0.24*	-6.61 ± 0.55*	-2.51 ± 0.62
T436A	5	-105.2 ± 2.2	1.69 ± 0.17	-4.00 ± 0.36	0.09 ± 0.46
A437V	6	-113.3 ± 3.5*	2.17 ± 0.32	-5.43 ± 0.64*	-1.48 ± 0.70
L438A	7	-110.4 ± 4.2*	1.52 ± 0.11*	-3.76 ± 0.26	0.33 ± 0.38
I439A	4	-78.9 ± 2.4*	1.60 ± 0.16	-2.83 ± 0.23*	1.27 ± 0.36
Q440A	10	-102.2 ± 2.6	1.73 ± 0.14	-3.95 ± 0.24	0.15 ± 0.37
S441A	7	-87.5 ± 2.9*	1.90 ± 0.11	-3.74 ± 0.19	0.36 ± 0.34
L442A	7	-91.8 ± 2.2*	1.70 ± 0.09	-3.53 ± 0.22	0.56 ± 0.36
D443A	6	-86.4 ± 3.6*	1.79 ± 0.18	-3.44 ± 0.24	0.65 ± 0.37

Table 2

basal cAMP		
$L = \beta/\alpha * L'$	α	0.0001594
	β	1198
$K = \delta/\gamma * K'$	γ	1086
	δ	106.4
	$z\beta = -z\alpha$	1.123
	$z\delta = -z\gamma$	0.8437
	a	0.2
	r	25.85
L' range		0.01 - 50
K' range		10^-25 - 10^6

2 mm cAMP		
$L = \beta/\alpha * L'$	α	0.0003785
	β	208.4
$K = \delta/\gamma * K'$	γ	13.33
	δ	86.66
	$z\beta = -z\alpha$	0.8974
	$z\delta = -z\gamma$	0.9621
	a	0.2
	r	25.85
L' range		0.1 - 50
K' range		10^-15 - 10^5

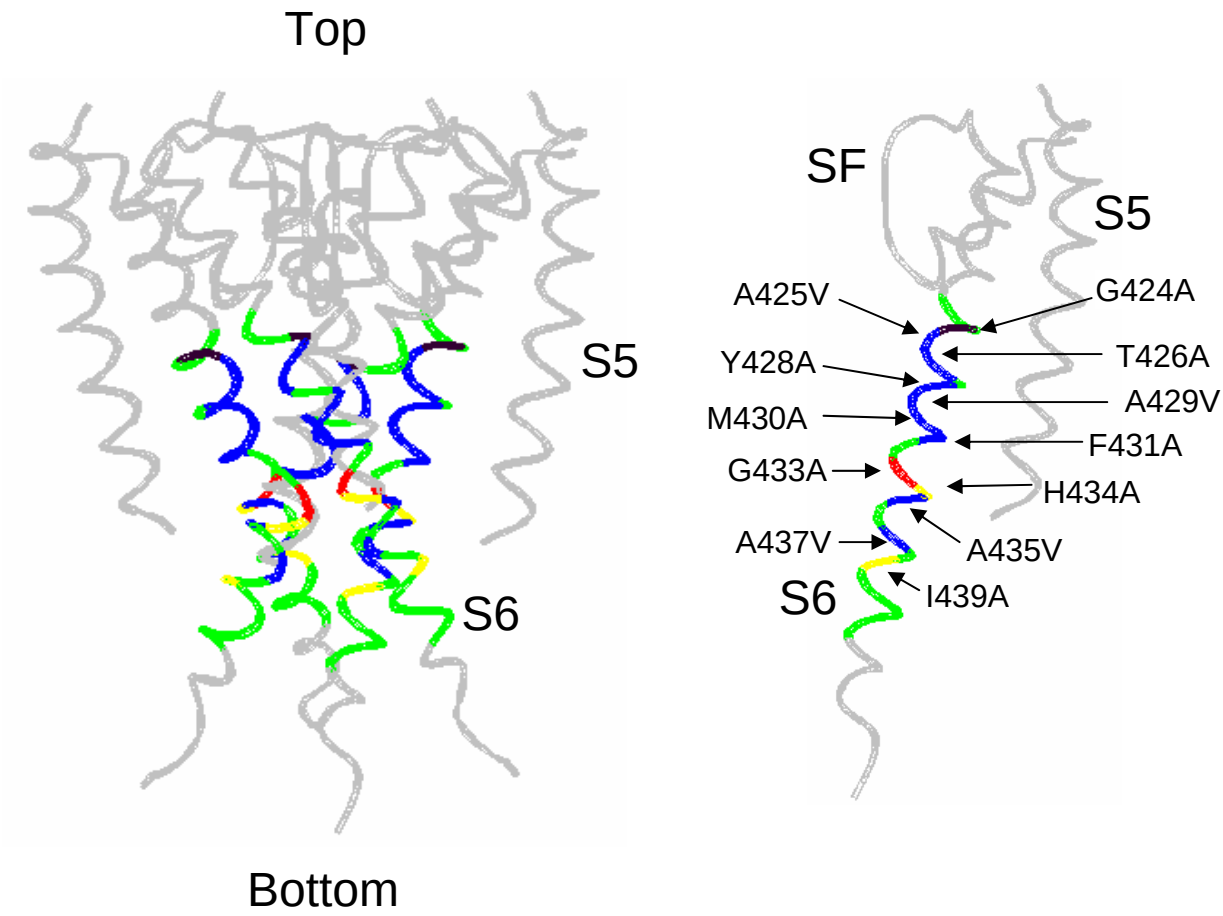

Supplementary Figure 1